



OPEN ACCESS

EDITED BY

Hussein M. El-Husseiny,
Tokyo University of Agriculture and
Technology, Japan

REVIEWED BY

Howard Dobson,
Invicro, United States
Nan Choisunirachon,
Chulalongkorn University, Thailand
Julia Grasiela Busarello Wolff,
Santa Catarina State University, Brazil

*CORRESPONDENCE

Mark Gray
✉ Mark.gray@ed.ac.uk

RECEIVED 12 September 2024

ACCEPTED 29 January 2025

PUBLISHED 26 February 2025

CITATION

Collie D, Cousens C, Wright S, Chang Z,
Meehan J, Brown H, Gray CD, MacGillivray TJ,
Griffiths DJ, Eckert CE, Storer N and
Gray M (2025) Spatial encoding and
growth-related change of sheep lung
radiomic features.

Front. Vet. Sci. 12:1495278.

doi: 10.3389/fvets.2025.1495278

COPYRIGHT

© 2025 Collie, Cousens, Wright, Chang,
Meehan, Brown, Gray, MacGillivray, Griffiths,
Eckert, Storer and Gray. This is an
open-access article distributed under the
terms of the [Creative Commons Attribution
License \(CC BY\)](https://creativecommons.org/licenses/by/4.0/). The use, distribution or
reproduction in other forums is permitted,
provided the original author(s) and the
copyright owner(s) are credited and that the
original publication in this journal is cited, in
accordance with accepted academic
practice. No use, distribution or reproduction
is permitted which does not comply with
these terms.

Spatial encoding and growth-related change of sheep lung radiomic features

David Collie¹, Chris Cousens², Steven Wright¹, Ziyuan Chang¹, James Meehan¹, Helen Brown¹, Calum D. Gray³, Tom J. MacGillivray⁴, David J. Griffiths², Chad E. Eckert⁵, Nicole Storer⁵ and Mark Gray^{1*}

¹The Roslin Institute, Royal (Dick) School of Veterinary Studies, University of Edinburgh, Edinburgh, United Kingdom, ²Moredun Research Institute, Pentlands Science Park, Penicuik, United Kingdom, ³Edinburgh Imaging Facility, Queen's Medical Research Institute, University of Edinburgh, Edinburgh, United Kingdom, ⁴Centre for Clinical Brain Sciences, College of Medicine and Veterinary Medicine, University of Edinburgh, Edinburgh, United Kingdom, ⁵Interventional Oncology, Johnson & Johnson Enterprise Innovation, Inc., New Brunswick, NJ, United States

Introduction: Different regions of the small ruminant lung exhibit variable susceptibility to specific lung pathologies. Such susceptibility may be reflected in regional lung radiomic features extracted from computed tomography (CT) images. In this study, we investigated whether region-specific variation in radiomic features exists in ovine lungs and whether these features remain stable over time.

Methods: Thoracic CT image datasets from 30 young adult sheep were subject to an image segmentation protocol directed at partitioning the lung into individual lobar and sub-lobar segments for radiomic feature analysis. After identifying and removing unstable, non-reproducible, and highly correlated features, 22 features remained and were used as input for principal component (PC) analysis.

Results: The significance of segment-related influence on PC scores was determined and visualised. For six sheep, successive CT images were acquired at monthly intervals for a period of 9 months in order to assess time-dependent variation in radiomic features. The results indicated that there was a significant difference in radiomic features derived from different lung segments. Visualisation of PC scores highlighted differences between caudodorsal and cranioventral lung, between lobar and sub-lobar segments, and suggested a bias towards one lung or the other. Significant changes in PC scores occurred over time. With few exceptions, largely similar changes occurred across all segments in this regard.

Discussion: Overall, our results indicate that although sheep lung radiomic features are influenced by the lung segment of origin, their variation over time is largely consistent throughout the lung. Such influence should be borne in mind when interpreting radiomic features and their changes over time.

KEYWORDS

lung, computed tomography, radiomic features, lobar variation, sheep

1 Introduction

Respiratory disease in cattle and sheep is usually caused by a variety of pathogens, both viral (bovine respiratory syncytial virus (BRSV), parainfluenza 3 (PI3), adenovirus, bovine viral diarrhoea virus (BVDV), and infectious bovine rhinotracheitis (IBR)) and bacterial (*Pasteurella multocida*, *Mannheimia haemolytica*, *Histophilus somni*, and *Mycoplasma bovis*). Bovine respiratory disease is estimated to cost the UK £60–80 million annually (1, 2) and the

EU €576 million (3), with losses related to mortality, treatment costs, and reduced performance both during and after the period of illness. In North America, bovine respiratory disease is the most prevalent and economically devastating health concern of the cattle industry with the overall cost to the industry estimated, in 1997, at over \$750 million per year (4). Global losses are estimated to be >\$3 billion/year (5).

Ruminants display a characteristic regional susceptibility to lung pathology. Indeed, the disease associated with *Pasteurella multocida* and *Mannheimia haemolytica* infection typically displays a cranioventral distribution with often a sharp line of demarcation between the affected tissue and grossly normal tissue located caudodorsally. Whilst gravitational influence on inhaled bioaerosols has been speculated to contribute to this distribution (6), a similar distribution of cranioventral lung lesions is seen following intravenous inoculation of calves with *Pasteurella haemolytica* (7). Furthermore, intravenous endotoxin administration in supine sheep results in atelectasis of dependent lung regions and an associated increase in cellular pulmonary metabolism (8, 9). This effect is assumed to be reflective of an influx and activation of inflammatory and immune cells. Therefore, in small ruminants, the cranioventral lung regions appear particularly susceptible to infection, whether from blood or airborne sources. Understanding the basis of such regional susceptibility would be a key factor in preventing or mitigating the impact of respiratory disease.

In contrast to the radiologic interpretation of lung disease, which is primarily based on a qualitative assessment of first-order features reflecting the extent of attenuation and recognising the morphological patterns that are often associated with signs, symbols, or naturalistic images (10), radiomic feature analysis extracts measures of the spatial relationships between pixel intensities. In particular, radiomic feature analysis offers the facility to quantify aspects of largely 'subvisual' image texture. Such measurements can potentially provide insight into the histology and biology of the associated tissue (11, 12). Radiomics is a rapidly evolving field, particularly in the area of characterisation and monitoring of lung cancer (13, 14), where measurements are of notable value in the context of predicting the malignant and metastatic potential of lung tumour nodules and the response to treatment (15–17).

Whilst associations between global measures of lung function and 'lung-wide' radiomic feature characteristics have been described (18), it is only more recently that the potential of radiomic feature analysis to quantify subregional pulmonary function has been explored (19). The latter study found that certain radiomic features (GLRLM run length non-uniformity and GLCM sum average) were highly correlated with functional imaging of regional ventilation. Subregions within the lung could also be described as habitats, acknowledging that variations in form and function do exist throughout the whole organ.

With the long-term goal of better understanding the factors underlying regional susceptibility to lung disease processes in small ruminants, we initially sought to address the primary hypothesis that radiomic features are spatially encoded in the healthy ovine lung. To this end, we developed an image characterisation workflow protocol to facilitate radiomic feature extraction. We used this to demonstrate region-specific variation in radiomic features and further demonstrated the stability of such features over time in growing sheep.

2 Materials and methods

2.1 Animals

Studies were performed under a UK Home Office Project Licence in agreement with the Animals (Scientific Procedures) Act 1986 and with consent from the University of Edinburgh Animal Welfare and Ethical Review Body. The recommendations for the welfare and use of animals in research were adhered to.

Details of the animals used, together with the overarching experimental design, are elaborated in a previous publication (20). Briefly, in addition to baseline computer tomography (CT) data obtained from 30 animals in order to verify lung health, data from CT scans repeated on a monthly basis over a period of 9 months were also obtained from six control animals from that cohort. Thirty young adult sheep (~4mo Texel cross mule; 39.2 ± 4.8 kg (mean \pm SD) of mixed sex (17 female and 13 male neutered) were commercially sourced. Sheep were housed on straw bedding under standard management conditions appropriate to a research setting. All imaging procedures were conducted under general anaesthesia, managed by veterinary specialist anaesthetists. Pre-anaesthetic medication, analgesics, induction, and maintenance of anaesthesia were performed as previously reported (20).

2.2 CT acquisition

A multislice SOMATOM Definition AS 64 slice helical CT machine was used to obtain thoracic CT scans (Siemens Healthcare Ltd., Erlangen, Germany) from each prone-positioned sheep. For six sheep, a further eight thoracic CT scans were acquired at monthly intervals to assess the nature and extent of time-dependent variation in radiomic features. An incremental continuous positive airway pressure (CPAP) protocol was applied to induce apnoea and standardise lung volume for CT.

2.3 Image processing

DICOM images were imported for segmentation in 3D Slicer software version 4.11.2.¹ Lungs were segmented by visual assessment using typical window threshold levels between $-1,024$ and -240 HU, with subsequent island selection and trimming as appropriate. Following airway segmentation (typical threshold levels between $-1,024$ and -900 HU), new segmentations were created and named according to the bronchial anatomy as described by Hare (21). The 3D paint facility was used to paint spheres centred on the relevant bronchi, and the 'grow from seeds' effect within the segment editor used the fast grow-cut method to simultaneously grow the spheres to neighbour boundaries within the lung segmentation. The radiomics module was applied to measure the radiomic features of the lung segments, selecting all features (resampled voxel size = 2,2,2, bin width = 64, enforced symmetrical

¹ www.slicer.org

TABLE 1 Radiomic features extracted using the radiomics module in Slicer.

| Feature Class | Features |
|--|--|
| First order | 10th percentile, 90th percentile, energy, entropy, interquartile range, kurtosis, maximum, mean absolute deviation, mean, median, minimum, range, robust mean absolute deviation, root mean squared, skewness, total energy, uniformity, variance |
| GLCM—Grey-level co-occurrence matrix | Autocorrelation, cluster prominence, cluster shade, cluster tendency, contrast, correlation, difference average, difference entropy, difference variance, inverse difference (Id), inverse difference moment (idm), inverse difference moment normalised (IDMN), inverse difference normalised (Idn), informational measure of correlation (IMC) 1, informational measure of correlation (IMC) 2, inverse variance, joint average, joint energy, joint entropy, maximal correlation coefficient (MCC), maximum probability, sum average, sum entropy, sum of squares |
| GLDM—Grey-level dependence matrix | Dependence entropy, dependence non-uniformity, dependence non-uniformity normalised, dependence variance, grey-level non-uniformity, grey-level variance, high grey-level emphasis, large dependence emphasis, large dependence high grey-level emphasis, large dependence low grey-level emphasis, low grey-level emphasis, small dependence emphasis, small dependence high grey-level emphasis, small dependence low grey-level emphasis |
| GLRLM—Grey-level run length matrix | Grey-level non-uniformity, grey-level non-uniformity normalised, grey-level variance, high grey-level run emphasis, long run emphasis, long run high grey-level emphasis, long run low grey-level emphasis, low grey-level run emphasis, run entropy, run length non-uniformity, run length non-uniformity normalised, run percentage, run variance, short-run emphasis, short-run high grey-level emphasis, short-run low grey-level emphasis |
| GLSZM—Grey-level size zone matrix | Grey-level non-uniformity, grey-level non-uniformity normalised, grey-level variance, high grey-level zone emphasis, large area emphasis, large area high grey-level emphasis, large area low grey-level emphasis, low grey-level zone emphasis, size zone non-uniformity, size zone non-uniformity normalised, small area emphasis, small area high grey-level emphasis, small area low grey-level emphasis, zone entropy, zone percentage, zone variance |
| NGTDM—Neighbouring grey tone difference matrix | Busyness, coarseness, complexity, contrast, strength |

First-order statistics describe the distribution of voxel intensities, grey-level co-occurrence matrix (GLCM) features quantify image texture by calculating how often pairs of pixels with specific values and in a specified spatial relationship to each other occur, grey-level dependence matrix (GLDM) features quantify grey-level dependencies defined by the number of connected voxels within a given distance that are dependent on the centre voxel, grey-level run length matrix (GLRLM) features quantify the occurrence of grey-level runs of consecutive pixels having the same value in a particular direction, grey-level size zone matrix (GLSZM) features quantify grey-level zones defined as the number of connected voxels that share the same grey-level intensity, and neighbouring grey tone difference matrix (NGTDM) features quantify the difference between a grey value and the average grey value of its neighbours within a certain distance.

GLCM) and saving the results to a file. Features used in subsequent analysis are indicated in Table 1. Radiomic feature maps were prepared using the graphical user interface developed by Kim et al. (22).

2.4 Assessment of reproducibility and stability

Reproducibility, defined by Tunali et al. (23) as the “consistency of a feature across image acquisition parameters such as patient position and respiration phase,” was assessed using paired thoracic CT image datasets acquired from one sheep before and after minor repositioning. Stability, defined as the “consistency of a feature across different segmentations,” was assessed by comparing feature measurements derived from separate segmentations applied to the same DICOM image series, from one sheep, and implemented by the same operator (DC) on two separate occasions. Features failing to demonstrate significant association between datasets were excluded from further analysis.

2.5 Removal of redundant features

In order to facilitate steps to reduce the dimensionality of the dataset, blocks of highly correlated variables (correlation coefficient > 0.95) were identified and redundant features were removed from each block to leave only one feature with the highest variance. The R corrplot package (24) was used for the correlation analysis.

2.6 Statistical analysis

Statistical analysis was conducted using Minitab (Minitab 20, www.minitab.com). Principal component analysis (PCA) was applied as an initial exploratory tool to determine the features contributing the most to respective principal components (PCs) and to assess whether anatomical disposition had a bearing on PC scores. PCA was applied to the z-score normalised radiomic features derived from each initial CT scan, and the PCs explaining the majority of the variance retained. ANOVA (mixed-effects model with sheep as a random factor and

segment as a fixed factor) was applied to the first PC to determine whether the segment explained a significant proportion of variance (25). Manual colour selection of Microsoft Excel conditional formatted PC score values and application to lung segmentations in Slicer facilitated the visualisation of PC score lung segmental distribution. In addition, segmentations representing caudodorsal to cranioventral lung slices were prepared and used to mask and crop lung volumes. These cropped volumes, exported in DICOM format, were used as input into the graphical user interface developed by Kim et al. (22), with a voxel region of interest of $3 \times 3 \times 3$, and radiomic feature classes selected as appropriate. In order to assess the time-dependent variation in PC scores for six sheep over the course of 9 months, the eigenvectors derived above were applied to the relevant z-score normalised radiomic features from the repeated data. One-way ANOVA was used to determine whether a significant change occurred over time for individual lung segments, and the correlation between PC scores derived from different lung segments was visualised through correlograms.

3 Results

3.1 Lung segmentation protocol

Visual appraisal of the results of the lung segmentation protocol is shown in Figure 1, where the pleural margins of the various lung segments can be discerned. The various segmental dispositions are largely consistent with the authors' experience in relation to segmental bronchoalveolar lavage procedures applied to ovine lungs post-mortem, where the expansion of those individual segments can be visualised (DC, personal communication).

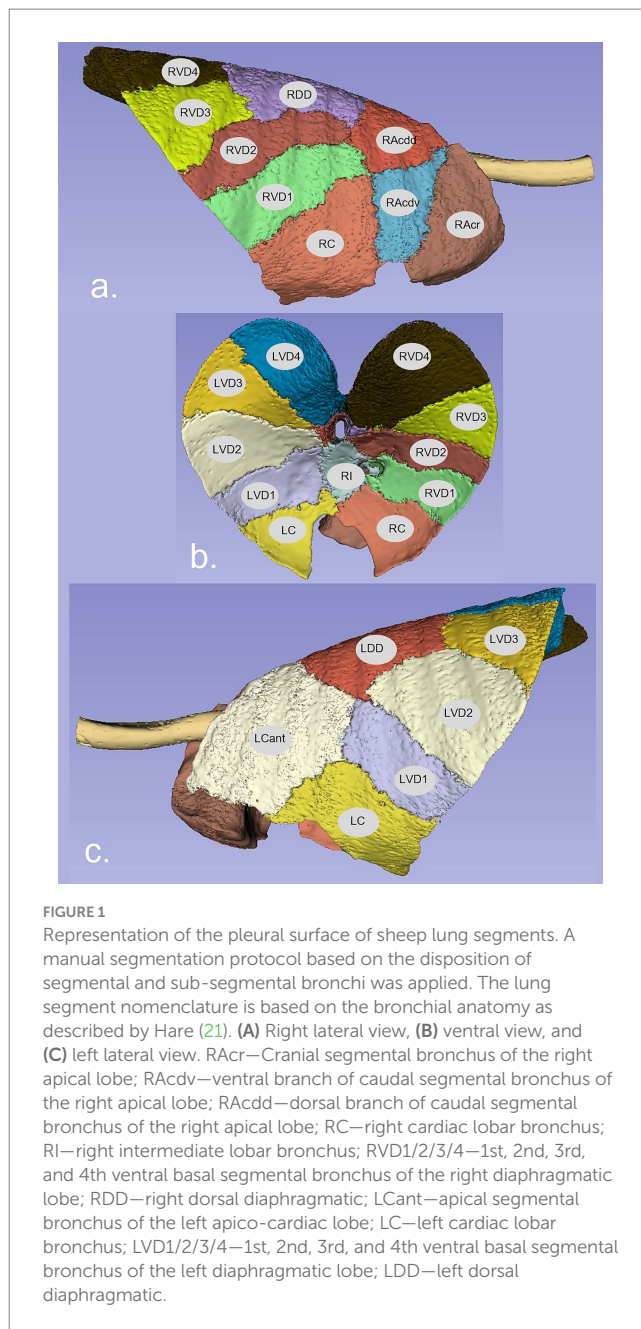
3.2 Reproducibility and stability

The radiomic features as listed in Table 1 proved consistent across different segmentations, with a median correlation of 0.94, and all features demonstrate a significant correlation ($p < 0.05$). Reproducibility of the features on two separate scans following minor repositioning proved less consistent (r^2 0.88) and 12 features failed to demonstrate a statistical association between repeat measurements on CT retake. Following their removal and the subsequent removal of features within the dataset that were highly correlated, a total of 22 features remained.

3.3 Principal component analysis

PCA applied to the 22 features using a correlation matrix indicated that 90% of the variance was explained by the first five components (PC1: 50%, PC2: 17%, PC3: 11%, PC4: 8%, and PC5: 4%). Examination of the PC1 vs. PC2 score plot suggested clustering on the first component axis according to whether segments were positioned dorsally (LDD, LVD3, LVD4, RDD, RVD3, and RVD4) or centrally (LCant, LVD1, LVD2, RI, RVD1, and RVD2) in the chest (Figure 2; abbreviations are as listed in the legend).

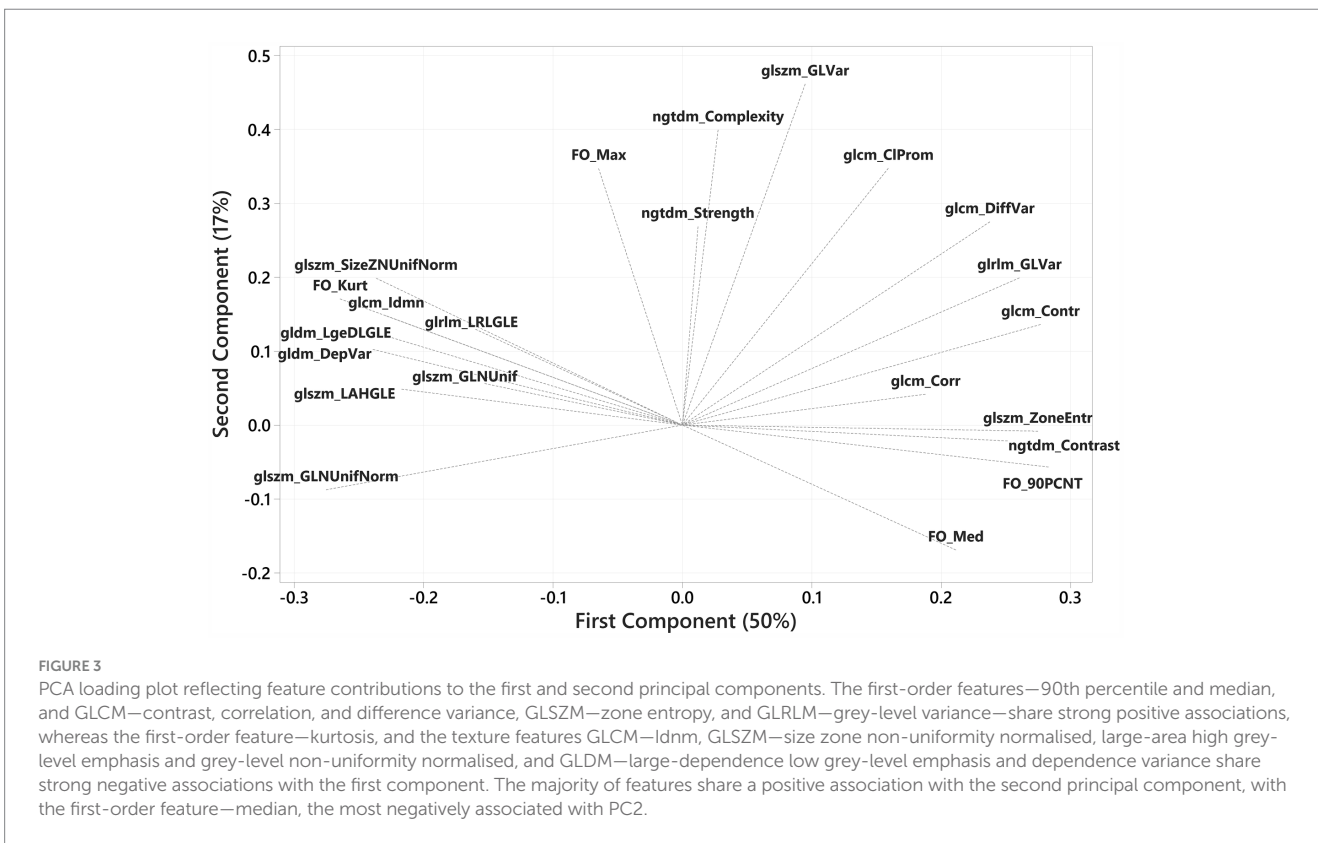
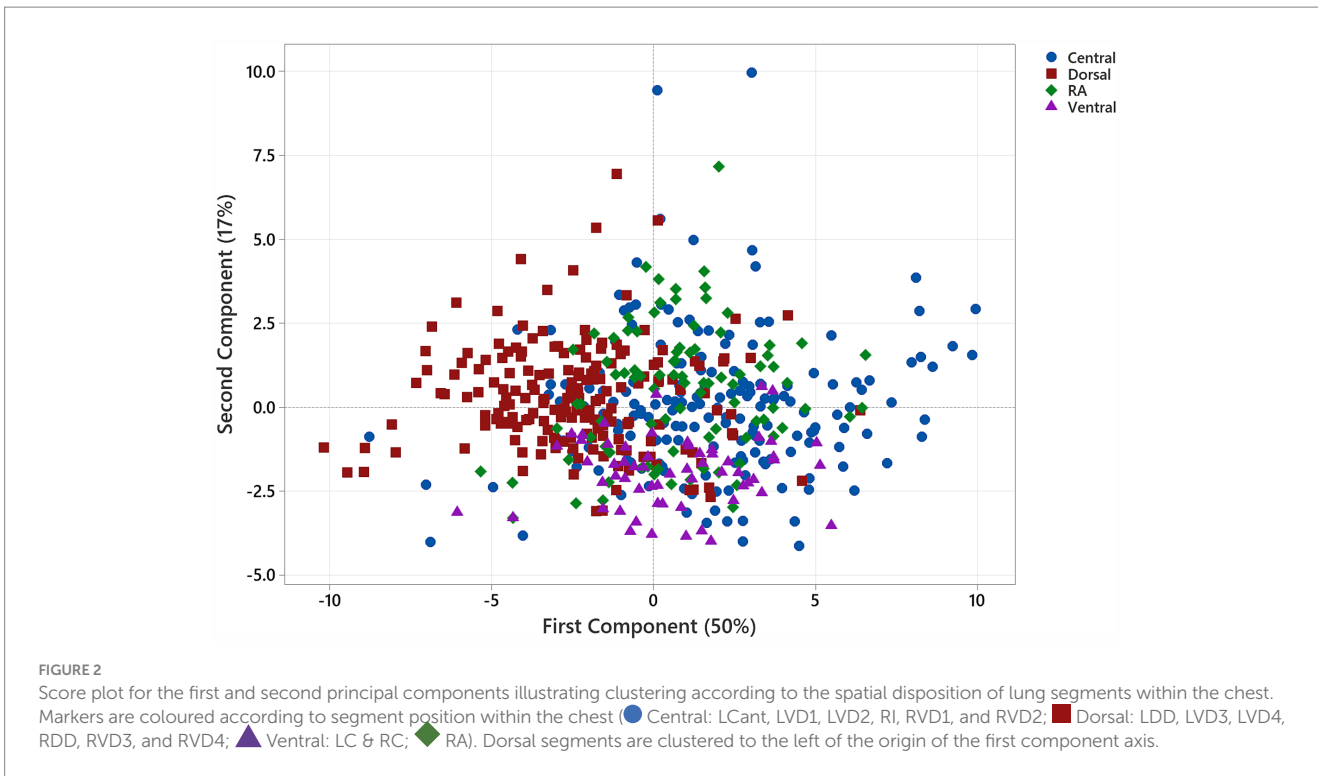
The loading plot for the first- and second-order components indicated that the first-order features—90th percentile and median, GLCM—contrast, correlation, and difference variance, GLSZM—zone entropy, and GLRLM—grey-level variance—shared strong positive



associations. In contrast, the first-order feature—kurtosis, and the texture features GLCM—Idnm, GLSZM—size zone non-uniformity normalised, large-area high grey-level emphasis and grey-level non-uniformity normalised, and GLDM—large-dependence low grey-level emphasis, and dependence variance—shared strong negative associations with the first component (Figure 3). The eigenvectors for the PCs are provided in Table 1.

3.4 Spatial encoding of radiomic features

The results of ANOVA applied to the first PC determined that at least one segment was different from the others ($p < 0.0001$), and the r^2 (adj) value indicated that the ANOVA model explained 77% of the variation in PC1 (Table 2).



Feature standardisation of the PC score data, sorting based on the scores, and applying conditional formatting to indicate the range and distribution of PC scores served to illustrate the influence of the segment on PC score values (Figure 4). The

anatomical disposition of these segmental PC scores is shown in Figure 5.

For the first PC, a gradient of increasingly positive values was apparent going from caudodorsal to cranioventral, with the most

TABLE 2 Eigenvectors from PCA.

| Feature class | Radiomic feature | PC1 | PC2 | PC3 | PC4 | PC5 |
|---------------|--|--------|--------|--------|--------|--------|
| First Order | 90th percentile | 0.283 | -0.057 | -0.115 | 0.014 | -0.152 |
| GLCM | Contrast | 0.277 | 0.136 | 0.025 | -0.033 | 0.184 |
| GLSZM | Zone entropy | 0.275 | -0.008 | -0.122 | 0.151 | 0.065 |
| GLRLM | Grey-level variance | 0.261 | 0.199 | 0.159 | 0.086 | -0.019 |
| NGTDM | Contrast | 0.251 | -0.022 | 0.276 | -0.003 | 0.068 |
| GLCM | Difference variance | 0.238 | 0.275 | 0.096 | -0.021 | 0.07 |
| First Order | Median | 0.211 | -0.169 | -0.268 | -0.101 | -0.213 |
| GLCM | Correlation | 0.188 | 0.042 | 0.232 | 0.308 | -0.5 |
| GLCM | Cluster prominence | 0.159 | 0.348 | 0.27 | 0.124 | -0.122 |
| GLSZM | Grey-level variance | 0.095 | 0.462 | 0.027 | 0.053 | 0.048 |
| NGTDM | Complexity | 0.028 | 0.399 | -0.345 | 0.045 | 0.19 |
| NGTDM | Strength | 0.012 | 0.269 | -0.065 | -0.544 | -0.244 |
| First Order | Maximum | -0.065 | 0.347 | -0.393 | 0.011 | -0.037 |
| GLSZM | Grey-level non-uniformity | -0.153 | 0.056 | -0.032 | 0.562 | 0.346 |
| GLRLM | Low grey-level run emphasis | -0.16 | 0.13 | 0.378 | -0.191 | 0.365 |
| GLSZM | Large-area high grey-level emphasis | -0.217 | 0.049 | -0.071 | 0.397 | -0.157 |
| GLCM | Inverse difference moment normalised | -0.229 | 0.148 | -0.304 | 0.047 | -0.182 |
| GLDM | Large-dependence low grey-level emphasis | -0.23 | 0.121 | 0.312 | -0.059 | -0.054 |
| GLSZM | Size zone non-uniformity normalised | -0.237 | 0.199 | 0.096 | -0.027 | -0.126 |
| GLDM | Dependence variance | -0.239 | 0.102 | 0.177 | 0.112 | -0.433 |
| First Order | Kurtosis | -0.265 | 0.171 | -0.007 | -0.103 | 0.034 |
| GLSZM | Grey-level non-uniformity normalised | -0.275 | -0.088 | 0.061 | -0.087 | 0.025 |

The eigenvectors are linear combinations of the original variables that essentially describe how each variable contributes to each principal component.

positive values present in RI, and some suggestion of a left-sided lung bias towards more positive PC score values. For PC2, cranial and craniodorsal positivity was noted, with markedly negative values in RC and LC. For PC3, strong positivity in RI was apparent, with marked dorsal (LDD and RDD) and craniodorsal (LCant) negativity. PC4 featured strong positivity in RAcr and positivity in RC, RDD, and LDD. For PC5, an increasingly positive value gradient was apparent going from caudodorsal to cranioventral in both lungs, with the most positive values present in LCant.

Visual appraisal of these gradients was made possible through the generation of the radiomic feature maps for variables with a major influence on the principal components. A feature map of GLCM contrast, the texture feature with the strongest positive association with PC1, is shown in Figure 6.

3.5 Growth-related change in radiomic features

In the six sheep studied at monthly intervals between 4 and 12 months of age, bodyweight increased from 37.7 ± 3.1 to 67.5 ± 4.8 Kg and measured lung volumes increased from $1,297 \pm 394$ to 1840 ± 195 cm³ (mean \pm SD).

The time-dependent dynamics of segment PC scores are shown in Figure 7. Analysing the significance of change between consecutive

CTs indicates that at times (in red) there was synchrony within the cohort of sheep; i.e., all six sheep demonstrated the same direction of change for the majority of segments (e.g., PC3 between CT1 and CT2, and between CT4 and CT5). The association between paired PC scores from different lung segments is illustrated in the correlograms in Figure 8. With the exception of LC for PC1 scores, there was generally a high degree of concordance between scores from different segments.

4 Discussion

In addressing our hypothesis, we used PCA to summarise the variation across the dataset and examined whether PCs would vary according to lung segment, reflecting a spatial 'encoding' of lung radiomic features. We demonstrated a region-specific increasing emphasis of PC1 from caudodorsal to cranioventral, with a positive bias towards the left lung, and RI notable as a positive extreme. A feature map prepared for GLCM contrast, the radiomic texture feature with the strongest positive association with PC1, confirmed this gradient. A marked decreasing dorsal to ventral gradient was noted for PC2 with particularly negative values for RC and LC. Regarding the observations that fuelled the central hypothesis, PC5 was notable for closely reflecting classic notions of respiratory pathology distribution associated with acute suppurative and acute fibrinous bronchopneumonia, as well as chronic bronchopneumonia (26). Such

lung pathologies are generally multifactorial and often encompass infection with *Mannheimia haemolytica*, *Pasteurella multocida*, *Histophilus somni*, and *Mycoplasma* spp. (26). Whilst analysis of individual features would have demonstrated similar associations, the functional or form-based underpinnings of either PCs or individual radiomic feature measurements are unknown, and investigation of such is beyond the scope of the present study. Therefore, for the purpose of addressing the hypothesis, we opted for the simplicity that PCA affords.

The bronchi serving RI and RC arise in common from the right main bronchus, with RI located in the mediastinal recess between the heart and diaphragm. It was occasionally noted that the margins of RI were poorly defined following the lung segmentation. Whilst this effect was partly a consequence of the close association of this segment with the caudal cardiac and cranial diaphragmatic cupola margins, it was also compounded by the segment's tendency towards increased attenuation relative to the other segments (RI -492 (-928, -15); remaining lung -646 (-794, -149); median (range) Hounsfield units).

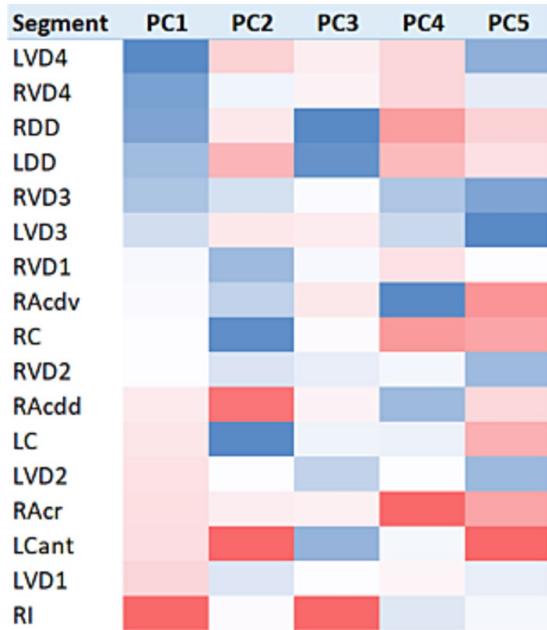


FIGURE 4 Heatmap visualisation of lung segment PC score data. Baseline (n = 30) PC scores were feature-standardised and conditionally formatted within columns to illustrate the intensity and range of values for each PC score. All columns are sorted on the basis of the first principal component.

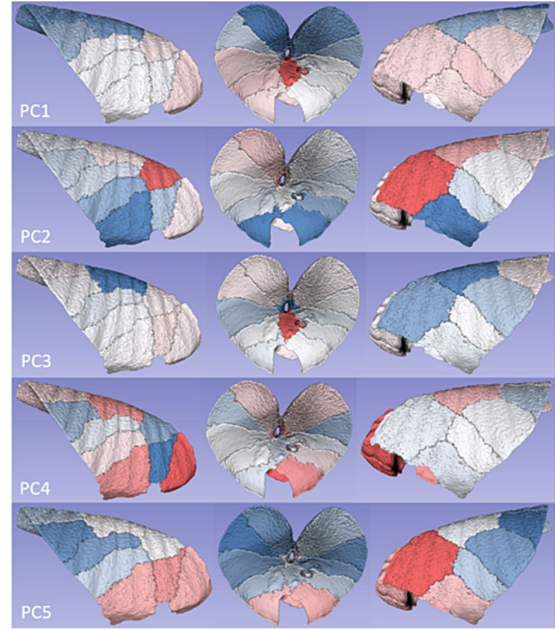


FIGURE 5 Segmental disposition of PC scores. Colour intensities from the heatmap in Figure 4 were ascribed to the respective segment volumes in order to illustrate the anatomical disposition of average principal component values.

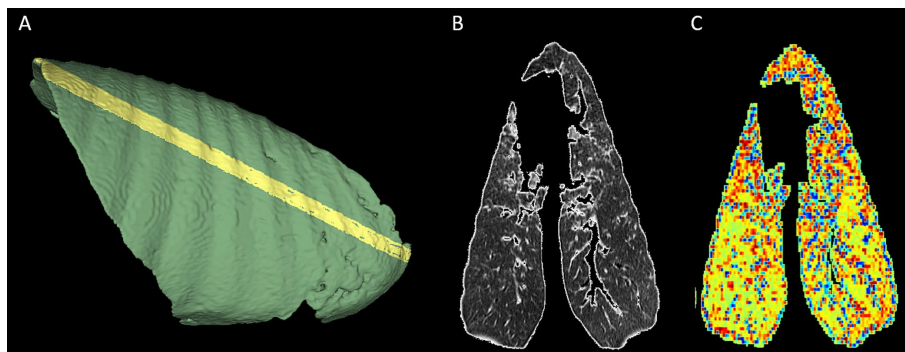
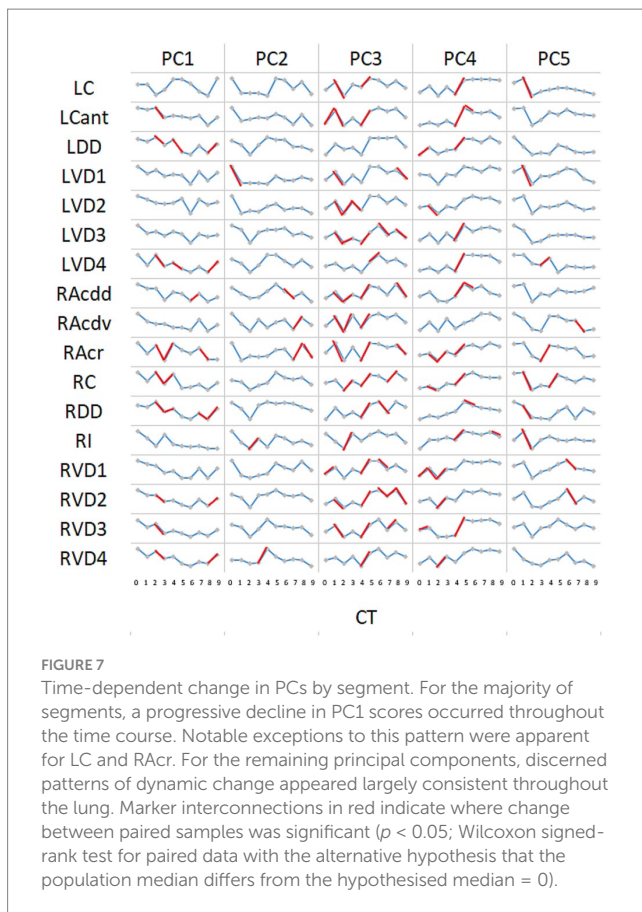


FIGURE 6 Feature map of *glcm_contrast*, demonstrating caudodorsal to cranioventral gradient. An oblique segmentation was created and used to mask and crop a randomly chosen lung volume from the cohort to facilitate radiomic feature map creation. (A) The oblique aspect of the segmentation is apparent on the pleural surface of the right lung. (B) The mid-slice CT image. (C) The related radiomic feature map for *glcm_contrast*. An increasing caudodorsal to cranioventral intensity gradient is apparent for this feature. In (B,C), the right lung is positioned on the right of the image, and the top of the image represents the cranial aspect.



Special emphasis was placed on evaluating RI segment boundaries, and where necessary, manually adjusting them to compensate for this effect. However, it should be noted that conducting the PCA without including the RI segment led to the same general conclusions regarding the spatial segmental disposition of the major PCs.

Whilst the present approach averaged lung segmental radiomic feature values, Yang et al. (19), by employing a 3D sliding window kernel to capture radiomic features for each voxel, were able to generate 3D feature maps that revealed subsegmental variation in radiomic features that were otherwise visually inapparent (19). Such an approach could potentially offer more focus on exploring the lung pathobiology underlying particular radiomic feature extremes in preclinical models, where tissue sampling could be specifically directed by radiomic feature analysis of CTs acquired immediately prior to euthanasia.

Since our results indicate that radiomic features vary across the normal ovine lung, the question arises as to which aspects of lung function or anatomy might be associated with such PC distribution and, conceptually, with disease susceptibility. Certainly, the proportion of air relative to tissue is reduced in dependent lung regions, a feature discernible in CT as increased attenuation (27–29). Furthermore, studies of ventilation and perfusion in the prone sheep lung indicate that dependent (ventral) regions are relatively poorly ventilated, whereas perfusion is preferentially distributed to dorsal regions (30). Regional lung compliance maps obtained from anaesthetised supine pigs also highlight increased compliance in dependent lung regions (31), and varying elastic behaviour of lung tissue according to gravitational influence (32).

Changes in the healthy lung microbiome are an inherent feature of diseases such as suppurative bronchopneumonia or fibrinous pneumonia in small ruminants. We have previously demonstrated the variability that can exist in the healthy sheep lung microbiome with craniocaudal clustering evident (33), likely reflecting region-specific biochemical and physical pressures shaping ecosystem ecologies. The availability of multimodal spatial omics technologies to analyse metabolites, histology, and gene expression across tissue regions (34) will help elucidate the underlying mechanisms shaping such relationships in lung health, and provide the foundation to understand disease susceptibility. As spatial radiomics offers the potential to characterise *in vivo* subregional lung features relevant to specific aspects of lung biology and function, it will be a significant partner in this regard.

We found that, with the notable exceptions of LC and RAcr, the majority of segments demonstrated a progressive decline in PC1 scores between 4 and 12 months of age, a period of time when measured lung volumes increased appreciably. In lambs, postnatal lung volume changes are rapid during the first 2 months of life, accommodating the growth of nearly half the number of alveoli found in adult sheep, as well as an increase in alveolar size. Thereafter, the rate of increase starts to plateau, with volume increases beyond 6 months of age being much more modest (35). In line with the overall growth in lung volume, the pulmonary capillary network continues to expand through adulthood (36). Changes in the mechanical properties of the lung are evidenced by studies in goats demonstrating growth-related increases in dynamic lung compliance and viscous work of breathing and a decrease in total pulmonary resistance between 20 and 550 days of age (37). Whilst it is not known whether the major PC is specifically influenced by any of these changes, it is, however, tempting to speculate that the progressive change in PC values does indeed reflect on some aspects of growth-related changes in lung structure and/or function.

For the remaining PCs, discerned patterns of dynamic change appeared largely consistent throughout the lung. In some instances (e.g., PC3 between CT1 and CT2 and between CT4 and CT5), the monthly patterns of change were consistent (i.e., demonstrated by every sheep in the group). These sheep were group housed within the same airspace and demonstrated no clinical signs suggestive of respiratory disease throughout the time course of the experiment. However, our analysis indicates that every sheep experienced the same pattern of change in their lung CT images at the same point in time. The radiomic features with the strongest positive association to PC3 were GLRLM low grey-level run emphasis, a measure of the distribution of low grey-level values, and GLDM large-dependence low grey-level emphasis, which reflects the grey-level relationship between a central pixel or voxel and its neighbourhood (Table 1). Both reflect low-resolution lung structure heterogeneity, i.e., coarse texture (38, 39). These healthy co-habiting animals experiencing similar subtle changes in lung image characteristics are significant and warrant further analysis. In particular, probing for associations with more sensitive indices of systemic and respiratory states, as well as air quality in the housing environment, such as the presence of particulates and bioaerosols (airborne viruses, bacteria, and fungi), would appear logical.

In conclusion, we used PCA to reduce a dataset of lung radiomic features derived from healthy sheep lung segments to

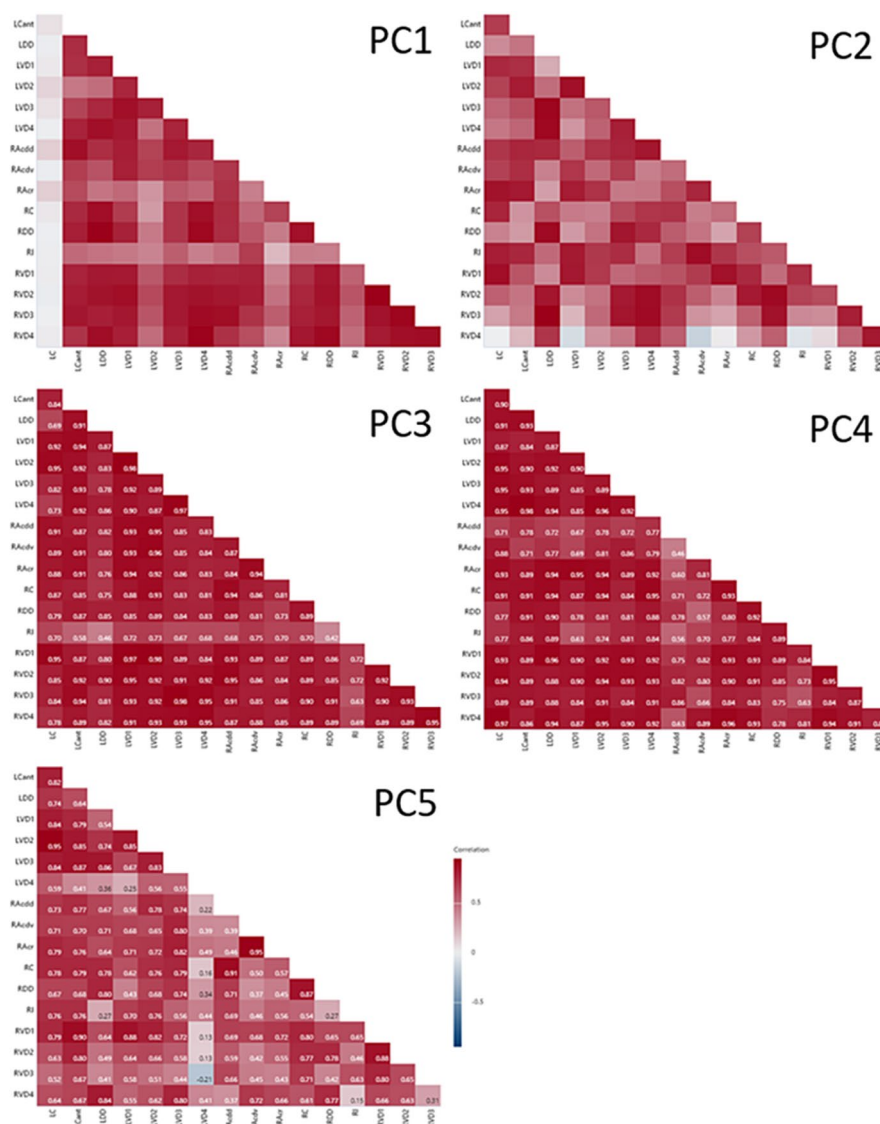


FIGURE 8
 Correlograms of segmental PC values paired by CT. With the exception of LC for PC1, there was generally good agreement between segments for PC scores paired within CTs.

five uncorrelated PCs explaining 90% of the total variance. We established that the PCs are spatially encoded in the sheep lung, demonstrating an increasing emphasis of the first component from caudodorsal to cranioventral, and a marked decreasing dorsal-to-ventral gradient for PC2. Furthermore, we demonstrated a time-dependent progressive decline in PC1 scores between 4 and 11 months of age. Whilst patterns of change for PCs were generally highly consistent between segments, indicating an organ-level response, deviation from this was observed for the left cardiac segment, indicating a local influence on radiomic features. Finally, at certain times we observed the same patterns of change in texture features in all sheep group-housed together, suggesting a shared subclinical lung response to an unknown stimulus. Our findings provide a baseline for understanding the nature and temporal variation of radiomic features in healthy sheep lungs. Such data will be central to interpreting radiomic feature

characteristics associated with disease and determining the extent of association between such changes and concomitant lung pathology.

Data availability statement

The raw data supporting the conclusions of this article will be made available by the authors, without undue reservation.

Ethics statement

The animal studies were performed under a UK Home Office Project Licence in agreement with the Animals (Scientific Procedures) Act 1986 and with consent from the University of

Edinburgh Animal Welfare and Ethical Review Body. The recommendations for welfare and use of animals in research were adhered to. The study was conducted in accordance with the local legislation and institutional requirements.

Author contributions

DC: Conceptualization, Formal analysis, Methodology, Writing – original draft. CC: Conceptualization, Funding acquisition, Writing – review & editing. SW: Conceptualization, Writing – review & editing. ZC: Conceptualization, Writing – review & editing. JM: Conceptualization, Writing – review & editing. HB: Formal analysis, Writing – review & editing. CG: Formal analysis, Writing – review & editing. TM: Formal analysis, Writing – review & editing. DG: Conceptualization, Writing – review & editing. CE: Conceptualization, Writing – review & editing. NS: Conceptualization, Writing – review & editing. MG: Conceptualization, Funding acquisition, Project administration, Resources, Writing – review & editing.

Funding

The author(s) declare that financial support was received for the research, authorship, and/or publication of this article. This work was supported by funding from Johnson & Johnson and the Scottish Government Rural and Environment Science and Analytical Services Division (RESAS). We acknowledge the financial support of the NHS Research Scotland (NRS), through the Edinburgh Clinical Research Facility for their support with the image analysis. DC received funding support from the Biotechnology and Biological Sciences Research Council (BB/

X010937/1, Prevention & Control of Infectious Diseases). CC and MG received a research grant from Johnson & Johnson to complete this study. The authors declare that this study received funding from Johnson & Johnson. The funder had no role in the collection, analysis, or interpretation of data or in the decision to publish the results.

Acknowledgments

Animal husbandry and anaesthesia were carried out and organised by the team at the Large Animal Research and Imaging Facility, University of Edinburgh. CT imaging was performed by diagnostic imaging staff from The Royal (Dick) School of Veterinary Studies, University of Edinburgh. We would like to express our gratitude to Roni Kirkpatrick and Stefano Guido, staff at BioResearch and Veterinary Services (BVS) at the University of Edinburgh, for their support in this project.

Conflict of interest

NS and CE are employees of Johnson & Johnson.

The remaining authors declare that the research was conducted in the absence of any commercial or financial relationships that could be construed as a potential conflict of interest.

Publisher's note

All claims expressed in this article are solely those of the authors and do not necessarily represent those of their affiliated organizations, or those of the publisher, the editors and the reviewers. Any product that may be evaluated in this article, or claim that may be made by its manufacturer, is not guaranteed or endorsed by the publisher.

References

- Hodgson C. (2010). New insights into the pathogenesis of acute bovine respiratory disease. In: Scientific, M. (ed.) Newsletter, Spring 2010.
- Scott P. (2016). Respiratory Disease in Dairy and Beef Rearer Units. Available at: <https://www.nadis.org.uk/4804> (Accessed August 1, 2024).
- Nicholas RA, Ayling RD. *Mycoplasma bovis*: disease, diagnosis, and control. *Res Vet Sci.* (2003) 74:105–12. doi: 10.1016/S0034-5288(02)00155-8
- Griffin D. Economic impact associated with respiratory disease in beef cattle. *Vet Clin North Am Food Anim Pract.* (1997) 13:367–77. doi: 10.1016/S0749-0720(15)30302-9
- Watts JL, Sweeney MT. Antimicrobial resistance in bovine respiratory disease pathogens: Measures, trends, and impact on efficacy. *Vet Clin North Am Food Anim Pract.* (2010) 26:79–88. doi: 10.1016/j.cvfa.2009.10.009
- Caswell JL, Williams KJ. Chapter 5 respiratory system In: Maxie G, editor. *Jubb, Kennedy & Palmer's Pathology of Domestic Animals*. 6th ed. Amsterdam: Elsevier (2016). p. 465–591.
- Thomas LH, Gourlay RN, Wyld SG, Parsons KR, Chanter N. Evidence that blood-borne infection is involved in the pathogenesis of bovine pneumonic pasteurellosis. *Vet Pathol.* (1989) 26:253–9. doi: 10.1177/030098588902600310
- Hinoshita T, Ribeiro GM, Winkler T, De Prost N, Tucci MR, Costa ELV, et al. Inflammatory activity in Atelectatic and normally aerated regions during early acute lung injury. *Acad Radiol.* (2020) 27:1679–90. doi: 10.1016/j.acra.2019.12.022
- Wellman TJ, De Prost N, Tucci M, Winkler T, Baron RM, Filipczak P, et al. Lung metabolic activation as an early biomarker of acute respiratory distress syndrome and local gene expression heterogeneity. *Anesthesiology.* (2016) 125:992–1004. doi: 10.1097/ALN.0000000000001334
- Chiarenza A, Esposto Ultimo L, Falsaperla D, Travali M, Foti PV, Torrisi SE, et al. Chest imaging using signs, symbols, and naturalistic images: a practical guide for radiologists and non-radiologists. *Insights Imaging.* (2019) 10:114. doi: 10.1186/s13244-019-0789-4
- Geady C, Keller H, Siddiqui I, Bilkey J, Dhani NC, Jaffray DA. Bridging the gap between micro- and macro-scales in medical imaging with textural analysis – a biological basis for Ct radiomics classifiers? *Phys Med.* (2020) 72:142–51. doi: 10.1016/j.ejmp.2020.03.018
- Tomaszewski MR, Gillies RJ. The biological meaning of Radiomic features. *Radiology.* (2021) 299:E256. doi: 10.1148/radiol.2021219005
- Song J, Yin Y, Wang H, Chang Z, Liu Z, Cui L. A review of original articles published in the emerging field of radiomics. *Eur J Radiol.* (2020) 127:108991. doi: 10.1016/j.ejrad.2020.108991
- Wu G, Jochems A, Refaee T, Ibrahim A, Yan C, Sanduleanu S, et al. Structural and functional radiomics for lung cancer. *Eur J Nucl Med Mol Imaging.* (2021) 48:3961–74. doi: 10.1007/s00259-021-05242-1
- Digumarthy SR, Padole AM, Gullo RL, Sequist LV, Kalra MK. Can Ct radiomic analysis in Nsclc predict histology and Egfr mutation status? *Medicine (Baltimore).* (2019) 98:e13963. doi: 10.1097/MD.00000000000013963
- Digumarthy SR, Padole AM, Lo Gullo R, Singh R, Shepard JO, Kalra MK. Ct texture analysis of histologically proven benign and malignant lung lesions. *Medicine (Baltimore).* (2018) 97:e11172. doi: 10.1097/MD.00000000000011172

17. Shi L, He Y, Yuan Z, Benedict S, Valicenti R, Qiu J, et al. Radiomics for response and outcome assessment for non-small cell lung Cancer. *Technol Cancer Res Treat.* (2018) 17:1533033818782788. doi: 10.1177/1533033818782788
18. Lafata KJ, Zhou Z, Liu JG, Hong J, Kelsey CR, Yin FF. An exploratory Radiomics approach to quantifying pulmonary function in Ct images. *Sci Rep.* (2019) 9:11509. doi: 10.1038/s41598-019-48023-5
19. Yang Z, Lafata KJ, Chen X, Bowsher J, Chang Y, Wang C, et al. Quantification of lung function on Ct images based on pulmonary radiomic filtering. *Med Phys.* (2022) 49:7278–86. doi: 10.1002/mp.15837
20. Cousins C, Meehan J, Collie D, Wright S, Chang Z, Todd H, et al. Tracking ovine pulmonary adenocarcinoma development using an experimental Jaagsiekte sheep retrovirus infection model. *Genes.* (2024) 15:1019. doi: 10.3390/genes15081019
21. Hare WCD. The broncho-pulmonary segments in the sheep. *J Anat.* (1955) 89:387–402.
22. Kim D, Jensen LJ, Elgeti T, Steffen IG, Hamm B, Nagel SN. Radiomics for everyone: a new tool simplifies creating parametric maps for the visualization and quantification of radiomics features. *Tomography.* (2021) 7:477–87. doi: 10.3390/tomography7030041
23. Tunalı I, Hall LO, Napel S, Cherezov D, Guvenis A, Gillies RJ, et al. Stability and reproducibility of computed tomography radiomic features extracted from peritumoral regions of lung cancer lesions. *Med Phys.* (2019) 46:5075–85. doi: 10.1002/mp.13808
24. Wei T., Simko V., Levy M., Xie Y., Jin Y., Zemla J. (2013). Corrplot: visualization of a correlation matrix. R package version 0.73, 230, 1–26.
25. Abapihi B, Adhi Wibawa GN, Baharuddin M, Agusrawati, Laome L. Anova on principal component as an alternative to Manova. *J Phys Conf Ser.* (2021) 1899:012103. doi: 10.1088/1742-6596/1899/1/012103
26. Mekibib B, Mikir T, Fekadu A, Abebe R. Prevalence of pneumonia in sheep and goats slaughtered at Elfora Bishoftu export abattoir, Ethiopia: a pathological investigation. *J Vet Med.* (2019) 2019:5169040. doi: 10.1155/2019/5169040
27. Millar AB, Denison DM. Vertical gradients of lung density in healthy supine men. *Thorax.* (1989) 44:485–90. doi: 10.1136/thx.44.6.485
28. Verschakelen JA, Van Fraeyenhoven L, Laureys G, Demedts M, Baert AL. Differences in Ct density between dependent and nondependent portions of the lung: influence of lung volume. *AJR Am J Roentgenol.* (1993) 161:713–7. doi: 10.2214/ajr.161.4.8372744
29. Wandtke JC, Hyde RW, Fahey PJ, Utell MJ, Plewes DB, Goske MJ, et al. Measurement of lung gas volume and regional density by computed tomography in dogs. *Investig Radiol.* (1986) 21:108–17. doi: 10.1097/00004424-198602000-00005
30. Richter T, Bellani G, Scott Harris R, Vidal Melo MF, Winkler T, Venegas JG, et al. Effect of prone position on regional shunt, aeration, and perfusion in experimental acute lung injury. *Am J Respir Crit Care Med.* (2005) 172:480–7. doi: 10.1164/rccm.200501-0040C
31. Perchiavazi G, Rylander C, Derosa S, Pellegrini M, Pitagora L, Polieri D, et al. Regional distribution of lung compliance by image analysis of computed tomograms. *Respir Physiol Neurobiol.* (2014) 201:60–70. doi: 10.1016/j.resp.2014.07.001
32. Pellegrini M, Derosa S, Tannoia A, Rylander C, Fiore T, Larsson A, et al. Effects of superimposed tissue weight on regional compliance of injured lungs. *Respir Physiol Neurobiol.* (2016) 228:16–24. doi: 10.1016/j.resp.2016.03.005
33. Glendinning L, Wright S, Pollock J, Tennant P, Collie D, Mclachlan G. Variability of the sheep lung microbiota. *Appl Environ Microbiol.* (2016) 82:3225–38. doi: 10.1128/AEM.00540-16
34. Vicari M, Mirzazadeh R, Nilsson A, Shariatgorji R, Bjärterot P, Larsson L, et al. Spatial multimodal analysis of transcriptomes and metabolomes in tissues. *Nat Biotechnol.* (2024) 42:1046–1050. doi: 10.1038/s41587-023-01937-y
35. Davies P, Reid L, Lister G, Pitt B. Postnatal growth of the sheep lung: a morphometric study. *Anat Rec.* (1988) 220:281–6. doi: 10.1002/ar.1092200308
36. Hislop AA, Pierce CM. Growth of the vascular tree. *Paediatr Respir Rev.* (2000) 1:321–8. doi: 10.1053/prrv.2000.0071
37. Bakima M, Lomba F, Lekeux P. Growth-related changes in the pulmonary function of goats. *Vet Res Commun.* (1990) 14:141–6. doi: 10.1007/BF00346554
38. Sun C, Wee WG. Neighboring gray level dependence matrix for texture classification. *Comp Vis Graph Image Proc.* (1983) 23:341–52. doi: 10.1016/0734-189X(83)90032-4
39. Xiaoou T. Texture information in run-length matrices. *IEEE Trans Image Process.* (1998) 7:1602–9. doi: 10.1109/83.725367